



Multi-purpose triboelectric-electromagnetic hybrid nanogenerator with a mechanical motion-controlled switch for harvesting low-frequency energy[☆]

Yan Zhang^{a,b}, Kangqi Fan^{a,b,*}, Jiuling Zhu^a, Shuxin Wu^a, Sheng Zhang^b, Tinghai Cheng^{b,**}, Zhong Lin Wang^{b,c,*}

^a School of Mechano-Electronic Engineering, Xidian University, Xi'an 710071, China

^b Beijing Institute of Nanoenergy and Nanosystems, Chinese Academy of Sciences, Beijing 101400, China

^c School of Materials Science and Engineering, Georgia Institute of Technology, Atlanta, GA 30332-0245, United States

ARTICLE INFO

Keywords:

Low-frequency motions
Triboelectric nanogenerator
Water waves
Mechanical motion-controlled switch
Energy harvesting

ABSTRACT

The renewable mechanical energy is pervasive but mainly contained in diverse, low-frequency and irregular motions, making its efficient exploitation highly difficult. Here, a multi-purpose triboelectric-electromagnetic hybrid nanogenerator (M-TEHG) is developed to tackle this issue through an ingenious mechanical motion-controlled switch (MMS). Consisting of a sprung-pendulum, a stiffness-adaptive plectrum and a slideable rotor, the MMS can not only transform low-frequency motions to one-way and high-speed spin but also enable the M-TEHG to automatically switch between non-contact state and contact state under the action of the rotor gravity. The M-TEHG exhibits frequency-multiplied outputs, improved durability, and superior adaptability to various motions. When triggered by low-frequency (≤ 5 Hz) swings and vibrations, the watch-sized M-TEHG can provide milliwatt-level electric power. When the M-TEHG is exposed to irregular water waves of around 1 Hz, the output power can reach roughly 0.7 mW. By harvesting human arm motions and water waves, the M-TEHG can power an electronic watch, drive a hygrometer, and light up 120 LEDs. This work provides a prospective strategy for tapping diverse low-frequency irregular motions as a green power source for wearable electronics and environment sensing systems.

1. Introduction

In the era of Internet of Things (IoT), a large number of widely distributed electronics are being connected into networks to exchange and process information anywhere and anytime [1,2]. With the rapid expansion of IoT, these battery-based electronics encounter two formidable challenges [3,4], one of which is the prohibitively high cost associated with the periodic renewal of numerous energy-limited batteries and the other is the potential environmental pollution caused by the fast-growing number of expired batteries. To address this issue, a renewable energy source is urgently demanded to continuously power these broadly dispersed electronics, break through the critical restraints of batteries, and hence sustain the long-term development of IoT. Among various renewable energy sources, the ambient mechanical

energy has attracted worldwide attention owing to its ubiquitous advantage and diverse transduction mechanisms [5–7]. The medium-high frequency vibrations and high-speed rotations have been converted into electricity by means of piezoelectric effect [5,8] and electromagnetic induction effect [9,10]. However, the dominant part of the ambient renewable mechanical energy is contained in low-frequency (< 5 Hz) and irregular motions (e.g., ocean waves [11], human limb swings [12], and track-induced vibrations [13]), for which piezoelectric generators suffer from frequency-mismatch induced low efficiency and electromagnetic generators are impaired by the slow change rate of the magnetic flux through pick-up coils.

Invented by Wang et al. in 2012 [14], triboelectric nanogenerator (TEHG) exhibits superior performance in harvesting low-frequency and irregular motions [15–17] and thus provides a desirable solution to the

[☆] Prof Zhong Lin Wang, an author on this paper, is the Editor-in-Chief of Nano Energy, but he had no involvement in the peer review process used to assess this work submitted to Nano Energy. This paper was assessed, and the corresponding peer review managed by Professor Chenguo Hu, also an Associate Editor in Nano Energy.

* Corresponding authors at: Beijing Institute of Nanoenergy and Nanosystems, Chinese Academy of Sciences, Beijing 101400, China.

** Corresponding author.

E-mail addresses: kangqifan@gmail.com (K. Fan), chengtinghai@binn.cas.cn (T. Cheng), zhong.wang@mse.gatech.edu (Z.L. Wang).

<https://doi.org/10.1016/j.nanoen.2022.107867>

Received 23 July 2022; Received in revised form 17 September 2022; Accepted 29 September 2022

Available online 3 October 2022

2211-2855/© 2022 Elsevier Ltd. All rights reserved.

sustainable powering of widely distributed electronics. Based on Maxwell's displacement current [18,19], TENG has diverse working modes and can generate very high output voltage through the conjunction of triboelectrification and electrostatic induction even at extremely low triggering frequencies [20–22], making it a parallel energy technology to the conventional electromagnetic generator [23,24]. With the predominant advantages of diverse material selection, simple structure, low cost, and lightweight, TENG has broad applications in nanoenergy [25–27], self-powered sensors [28–30], and large-scale blue energy [31–33]. So far, a series of TENGs have been developed to harvest ambient low-frequency mechanical motions, but most of them work at a frequency close to the low motion frequency, leading to sparse electric pulses and thus low effective power. The primary cause is the lack of a multi-purpose motion modulation mechanism that can transform low-frequency and irregular motions to one-way and high-speed spin to multiply the output frequency.

Another technical hurdle for TENG in the tapping of low-frequency motions is the low mechanical durability and electrical stability. To generate high electric outputs, close contact and rubbing between tribo-materials are required to maximize the contact electrification effect. However, the rubbing between tribo-materials may lead to severe material abrasion and thus gradually deteriorating output performance [32,34]. The non-contact TENGs can avoid the direct rubbing between tribo-materials, but the gradual dissipation of charges preserved on the dielectric tribo-layers also brings about diminishing electric outputs. To solve this dilemma, the soft contact design (using flexible materials [35, 36] or rabbit furs [37,38] as the dielectric tribo-layers) and working mode transition strategy (switching between contact mode and noncontact mode) [39,40] have been proposed, but they require continuous and strong driving forces (e.g., strong wind) to work, which the low-frequency and irregular motions cannot provide. Therefore, even if the transformation of low-frequency motions to high-speed spin could be implemented, an approach that can reduce the material abrasion without high demands for driving forces is still desired for rotary TENGs to achieve high mechanical durability and electrical stability under low-frequency and irregular motions.

Contrary to the large current but small voltage of electromagnetic generators (EMGs), the TENG has a high voltage and low current output under low frequency/speed conditions [23,41]. A hybrid generator obtained by integrating the two transduction mechanisms in one device can not only generate more electricity from one motion but also provide high voltage output (from the TENG) and large current output (from the EMG) [41–43]. In view of that the electricity converted from ambient mechanical energy is generally accumulated in capacitors to power electronics when the required voltage level is reached, the comparatively large current from the electromagnetic part of a hybrid generator can establish an infrastructural voltage level, based on which higher voltage of the capacitor can be achieved more quickly by the TENG part. Despite the distinctive advantages of a triboelectric-electromagnetic hybrid generator (TEHG), the challenge is how to ensure the simultaneous work of the two parts under the same motion.

In this paper, we report a multi-purpose TEHG (M-TEHG) that is realized with an ingenious mechanical motion-controlled switch (MMS) to efficiently harvest low-frequency vibrations, swings, and water waves. Consisting of a sprung-pendulum, a plectrum and a rotor, the MMS can transform low-frequency and irregular motions to one-way and high-speed spin, enabling the M-TEHG to generate frequency-multiplied electric outputs. With a tiny interspace between the rotor and supporting shaft, the M-TEHG can automatically transition between noncontact mode (NC-mode) and contact mode (C-mode) under the action of the rotor gravity, contributing to improved mechanical durability. A watch-sized M-TEHG can generate high output power of 8.78 mW, 4.85 mW, and 0.693 mW from low-frequency vibrations (5 Hz), swings (4 Hz), and water waves (1 Hz), respectively. The M-TEHG has also been used to successfully power an electronic watch, drive a hygrometer, and light up dozens of LEDs by harvesting human arm swings

and water waves, demonstrating broad applications in self-sustained wearable electronics and maintenance-free environment monitoring systems.

2. Results and discussion

2.1. M-TEHG configuration and working principle

The M-TEHG is developed to harness ambient low-frequency mechanical energy, such as the energy contained in human limb swings, ocean waves, and bridge vibrations, as shown in Fig. 1a. The electricity generated by M-TEHG (Figs. 1b and S1), after being rectified and accumulated in capacitors, has broad applications in wearable electronics, lighting electronics, and environment monitoring devices, as shown in Fig. 1c. The M-TEHG consists of a coaxially assembled pendulum and rotor, a disk-shaped electrode plate, and sixteen radially-arrayed pick-up coils, all of which are packaged in a watch-shaped housing with a circular lid. The pendulum includes a fan-shaped substrate with embedded mass blocks to tune its rotary inertia. A spiral spring is mounted between the pendulum and the lid to store the clockwise swing energy of the pendulum to enlarge the driving force for the anticlockwise spin of the rotor. A stiffness-adaptive bistratal plectrum is fixed to the pendulum to drive the rotor. The rotor with jagged inner wall comprises sixteen radially-arrayed magnets and three fan-shaped Fluorinated Ethylene Propylene (FEP) films, which enables the power generation through the triboelectric effect and the electromagnetic induction principle concurrently from the same motion (i.e., the spin of the rotor). The electrode plate anchored to the inner bottom of the housing includes six fan-shaped copper electrodes, forming two complementary electrode networks. The radially-arrayed pick-up coils each with 150 turns of varnished wire are connected in series and attached to the inside wall of the housing.

The M-TEHG first converts ambient low-frequency motions to (two-way) swing of the pendulum, and the latter enables the anticlockwise spin of the rotor through the stiffness-adaptive bistratal plectrum, as shown in Fig. 1d. Due to the one-way and rapid spin of the rotor, electric outputs can be generated simultaneously from both the triboelectric unit (FEP films and electrodes) and the electromagnetic unit (magnets and coils) with frequencies far larger than the excitation frequency, engendering enhanced output performance. Since the pendulum accelerates the rotor only during its anticlockwise swing, a spiral spring is employed to store the clockwise swing energy of the pendulum and release the stored energy to drive the rotor when the pendulum swings anticlockwise. Therefore, the introduction of the spiral spring contributes to the utilization of the entire stroke energy of the pendulum, which is conducive to the performance improvement of the M-TEHG.

In the M-TEHG, the motion modulation, i.e., transforming the swing of the pendulum to one-way spin of the rotor, is realized through a bistratal plectrum, as illustrated in Figs. 2a and S2. To exhibit this process, we calculated the stiffness of the plectrum under different conditions, as shown in Fig. S3 and elaborated in Supplementary Note 1. When the pendulum is triggered by ambient motions to swing anticlockwise, the plectrum moves along with the pendulum and spins the rotor in the same direction. In this case, the (forward) stiffness K_1 of the plectrum is large owing to the strengthening effect of the rigid layer, which can be determined by

$$K_1 = \frac{12EI}{\sin \varphi [4L_E^3 - L_R(3L_E - L_R)^2]} \quad (1)$$

where E , I , and L_E are respectively the Young's modulus, area moment of inertia, and length of the elastic layer; L_R is the length of the rigid layer; φ is the dip angle of the plectrum.

When the pendulum swings clockwise with respect to the rotor, the elastic layer of the plectrum detaches from the rigid layer and slides on the inner wall of the rotor. The (backward) stiffness K_2 of the plectrum in

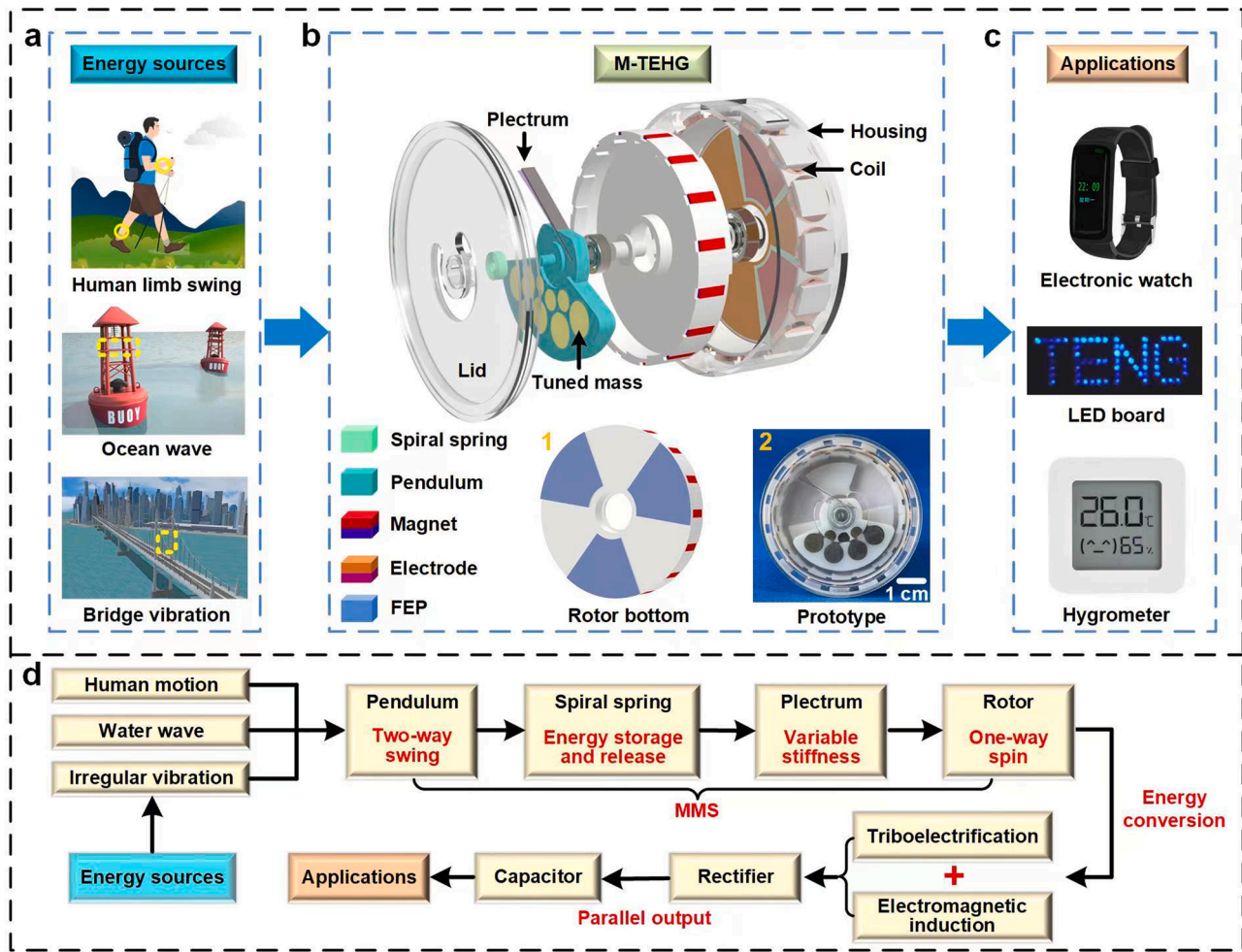


Fig. 1. Structure and application scenarios of the M-TEHG. (a) Exploitable energy sources by the M-TEHG. (b) Exploded view of the M-TEHG. Inset 1 demonstrates the FEP films arranged on the bottom of the rotor. Inset 2 is a picture showing the fabricated prototype. (c) Potential applications of the M-TEHG. (d) Working process of the M-TEHG.

this case depends only on the elastic layer, i.e.,

$$K_2 = \frac{3EI}{L_E^3} \quad (2)$$

Without the reinforcing effect of the rigid layer, the backward stiffness K_2 of the plectrum is largely reduced as compared with the forward stiffness K_1 , as shown in Fig. S3.

It can be seen from the above analysis that the plectrum can automatically switch its stiffness between K_1 and K_2 in accordance to the relative motion between the pendulum and the rotor. The motion modulation can be achieved if $K_1 \gg K_2$, which requires $L_E - L_R < L_E$. Moreover, mounting the plectrum on the pendulum with a dip angle φ can not only significantly increase the forward stiffness K_1 but also reduce the deflection ΔL of the elastic layer required to make the plectrum slide on the inner wall of the rotor (Fig. S3). The method for determining ΔL is given in Supplementary Note 1 [44]. With a sufficiently large forward stiffness, very small backward stiffness, and tiny deflection of the elastic layer, the one-way spin of the rotor can be realized by the pendulum and the stiffness-adaptive plectrum.

In the M-TEHG, the bearing used for assembling the rotor has an inner ring diameter slightly larger than the diameter of the supporting shaft. This design allows the rotor to move along the spin axis and switch between C-mode and NC-mode. If the spin axis of the M-TEHG tilts rightward, the rotor will move toward the electrode plate under the action of the gravity and make the M-TEHG work in C-mode, as illustrated in Fig. 2b. In this mode, the FEP is negatively charged while the

Cu electrode is positively charged owing to the triboelectric effect [45], as shown in the right panel of Fig. 2c. As the rotor spins, the negatively charged FEP will drive positive charges to flow back and forth between the two electrodes via the external circuit and electric load, converting the mechanical energy of the rotor into electric energy. On the contrary, if the spin axis of the M-TEHG tilts leftward, the rotor will move away from the electrode plate and thus the M-TEHG shifts into NC-mode. Enabled by the electrostatic induction, positive charges can also flow between the two electrodes through the external circuit to follow the motion of the negatively charged FEP, as illustrated in the left panel of Fig. 2c. The electrical potential distributions of the triboelectric unit in the two working modes are also calculated and given in Fig. S4 to show the potential difference between the two electrodes, which is the origin of the charges flowing in the external circuit. The electromagnetic unit works on the basis of the electromagnetic induction principle, as illustrated in Fig. 2d. When the magnet rotates along with the rotor and sweeps over the coil, the magnetic flux through the coil first grows and then declines, inducing the electric current in the coil to produce such a magnetic field that resists the variation of the magnetic flux through the coil. As a result, the induced current changes its direction when the magnet sweeps over the coil. Due to the circular and periodical arrangement of the magnets on the rotor, when one magnet moves away from the coil, the adjacent magnet starts to sweep over the coil and engender induced current in the coil again. As the rotor spins, this process repeats and alternating current can be produced continuously by

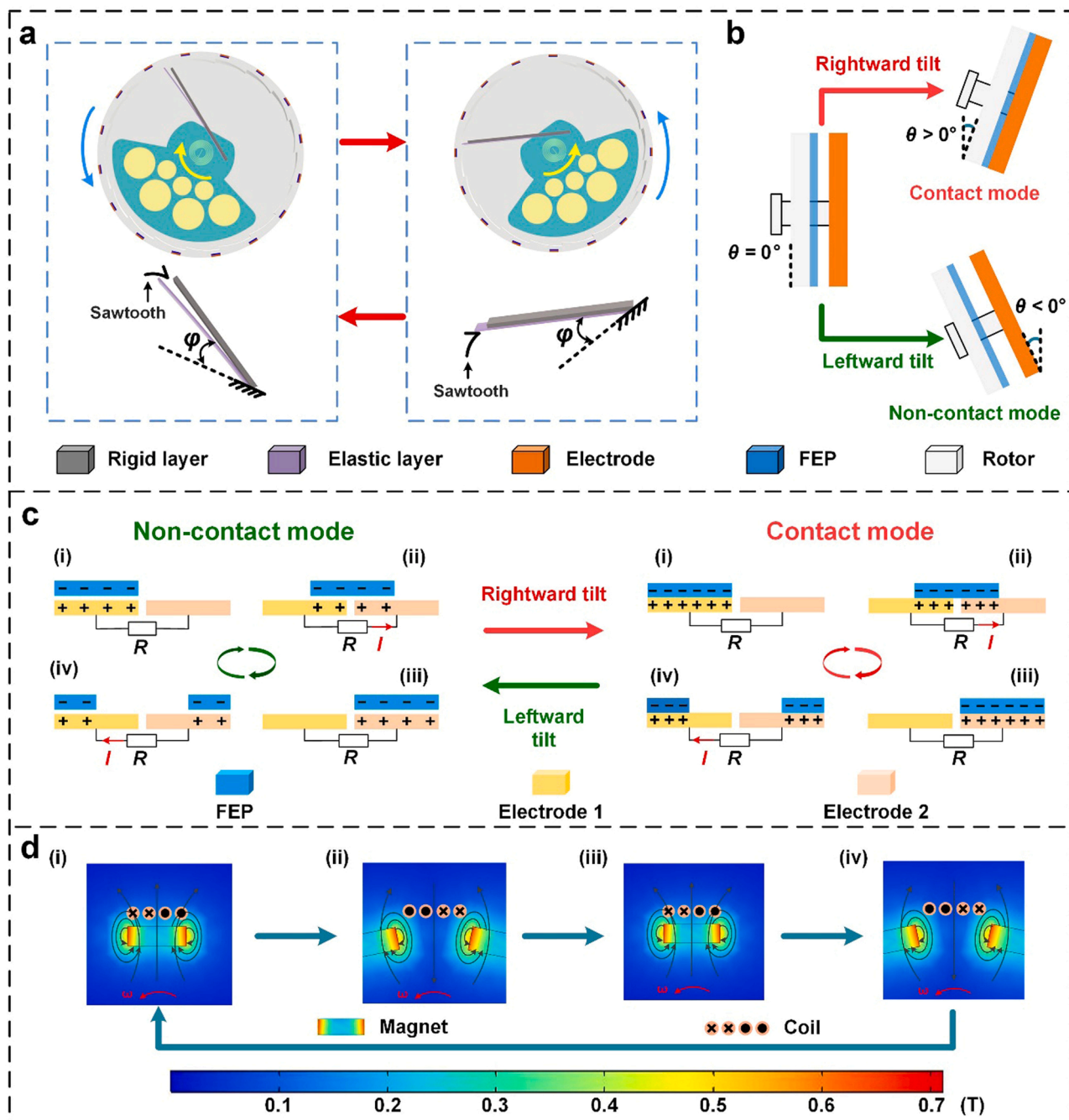


Fig. 2. Schematic diagram of the M-TEHG. (a) Transformation of the two-way swing of the pendulum to one-way spin of the rotor. (b) Working modes under various title angles of the spin axis. (c) Schematic working principle of the triboelectric unit under C-mode and NC-mode. (d) Schematic working principle and simulated magnetic flux distribution of the electromagnetic unit.

the electromagnetic unit.

To achieve the highest output performance, rotary TENGs are normally designed to work in C-mode to maximize the triboelectrification effect [46–48]. Due to the rubbing between tribo-materials, the C-mode TENG suffers from severe material abrasion, low mechanical durability, and unstable electric outputs [38]. Moreover, overcoming the friction resistance of C-mode TENGs requires strong driving forces [2], which ambient low-frequency and irregular motions can scarcely provide. The material abrasion and friction resistance can be addressed by setting the TENG work in the NC-mode. However, without direct contact between tribo-materials, the charges preserved on the surfaces of dielectric materials fade away, leading to degenerative output performance [34]. One ideal solution to this issue is the working mode transition (WMT)

strategy, by which the TENG works predominantly in NC-mode to avoid material abrasion and friction resistance and intermittently transitions into C-mode to replenish the dissipated charges through the triboelectrification effect [32,36,39]. For the M-TEHG that works normally with its spin axis parallel to the ground, although the rotor can move along its axle, it works mainly in the NC-mode because a tiny contact force induced in the C-mode can push the rotor away from the electrode plate and force the M-TEHG back into the NC-mode. In view of the fact that ambient motions are generally irregular, unstable, and direction-inconstant, the spin axis of the M-TEHG will probably tilt leftward and rightward alternately in practical applications, making the M-TEHG intermittently switch between C-mode and NC-mode. As a result, the automatic WMT can be realized through the utilization of the

irregularity and instability of practical motions to improve the long-term durability and stability of the triboelectric unit. The WMT of the M-TEHG is exhibited in Supporting Video S1 and Fig. S5. When the human arm swings with the spin axis of the M-TEHG tilting leftward, the device works in NC-mode, leading to comparatively low electric output. On the contrary, if the device swings with its spin axis tilting rightward, it works in C-mode, bringing about significantly high electric output. Due to the irregularity of practical low-frequency motions, such as human arm swings, the working modes of the M-TEHG can be switched automatically and intermittently. The WMT condition and the improved durability of the M-TEHG are elaborated in the next section.

2.2. Demonstration of motion modulation by MMS

Although the ambient mechanical energy is abundant, its direct conversion into electricity is normally inefficient due to the irregularity, instability and low occurring frequency [49]. For example, the pendulum-based generators can only respond to ambient motions at low frequencies due to the two-way swing of the pendulum with small angles and low speeds [50–52], leading to low output power (< 0.1 mW). The M-TEHG overcomes this limitation via the motion modulation strategy implemented by an innovative MMS. To examine the feasibility and effectiveness of this strategy, we used both a stepper motor and a swing arm to actuate the M-TEHG to observe the output characteristics of the triboelectric unit.

When the pendulum of the M-TEHG is driven directly by a stepper

motor at 4 Hz, the measured open-circuit voltage (OC-voltage) V_{OC} and short-circuit current (SC-current) I_{SC} of the triboelectric unit are shown in Fig. 3 along with the spin speed ω of the rotor, which demonstrate the successful transformation of two-way swing of the pendulum to one-way spin of the rotor. For tilt angle $\theta \leq -30^\circ$, the M-TEHG works in NC-mode and generates almost constant electric outputs ($V_{OC} = 50$ V and $I_{SC} = 0.3$ μ A) under a comparatively small swing amplitude of $\alpha = 60^\circ$, as shown in Fig. 3a, b. If θ varies between -10° and 0° , the horizontal tremor of the rotor due to the minute interstice between the bearing and the shaft takes effect, which brings about the occasional sliding contact or rubbing between the rotor (FEP films) and electrodes and hence gradually increased V_{OC} and I_{SC} . For $\theta > 0^\circ$, the M-TEHG works all the way in C-mode and the contact force F_C between the FEP film and the electrode can be calculated as

$$F_C = Mg \sin \theta \quad (3)$$

where M represents the effective mass of the rotor and $g = 9.8$ m/s² is the acceleration of gravity. It is apparent that F_C is positively related to θ in the range from 0° to 90° . Due to the enhanced triboelectric effect with the enlarged contact force, electric outputs of the triboelectric unit grow continuously with increasing θ from 0° and reach the saturated values ($V_{OC} = 200$ V and $I_{SC} = 1.4$ μ A) when $\theta \geq 60^\circ$. Electric outputs of the triboelectric unit are attributed to the transformation of the swing of the pendulum to the spin of the rotor, as shown in Fig. 3c, where the spin/swing speed is measured at $\alpha = 60^\circ$ and $\theta = 0^\circ$, and the pendulum speed herein represents the anticlockwise rotary speed of the stepper motor.

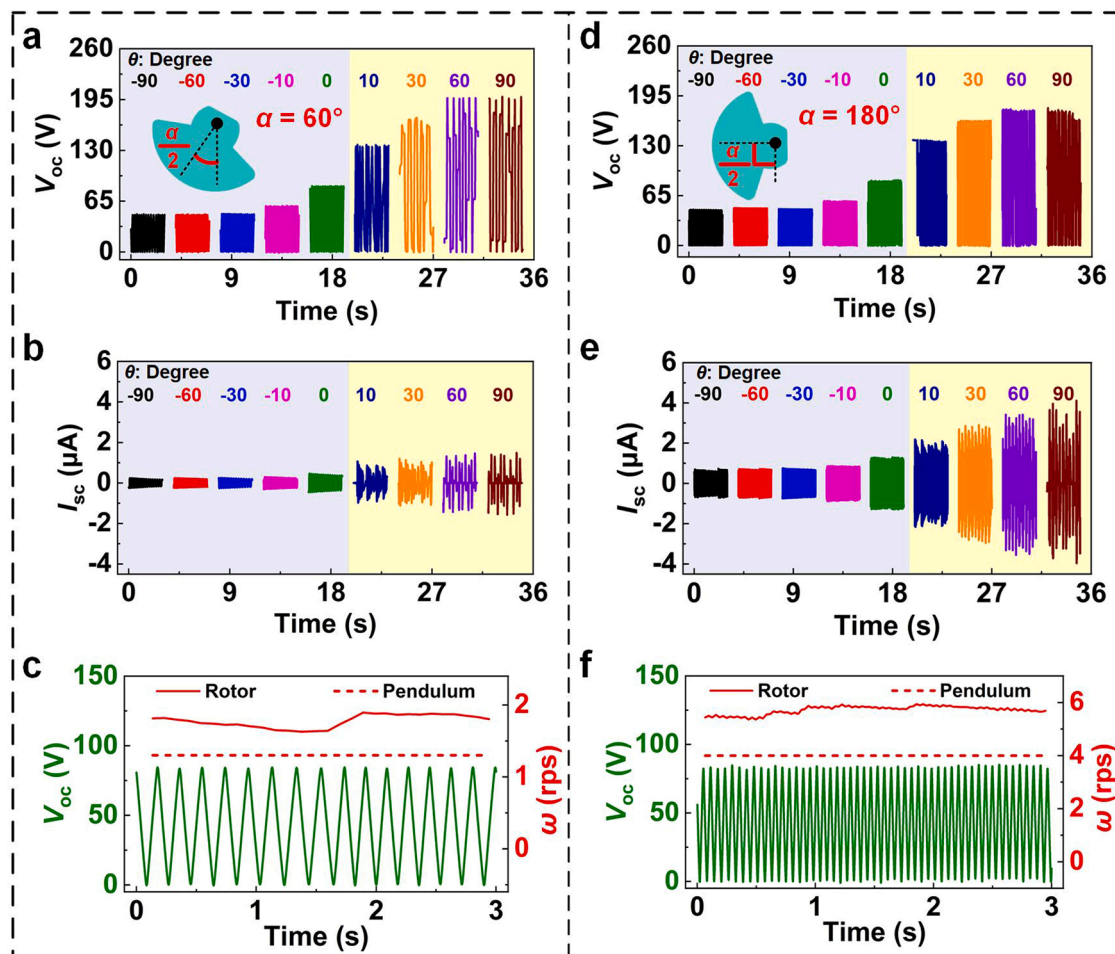


Fig. 3. Demonstration of transforming two-way swing to one-way spin by the MMS when the pendulum is driven directly by a motor. (a) OC-voltage and (b) SC-current under various tilt angles for $\alpha = 60^\circ$. (c) OC-voltage, rotor spin speed and pendulum swing speed for $\alpha = 60^\circ$ and $\theta = 0^\circ$. (d) OC-voltage and (e) SC-current under various tilt angles for $\alpha = 180^\circ$. (f) OC-voltage, rotor spin speed and pendulum swing speed for $\alpha = 180^\circ$ and $\theta = 0^\circ$.

this test, the pendulum moves synchronously with the motor since it is driven directly by the shaft of the motor. The motor was programmed to rotate bi-directionally with an almost constant speed except the transient reversing process (~ 0.03 s), as shown in Fig. S6. Since the rotor in the M-TEHG spins anticlockwise, the anticlockwise speed of the pendulum, which is equal to the anticlockwise rotary speed of the stepper motor, is chosen to make a comparison between the rotor and the pendulum.

If the swing amplitude α is increased to 180° , electric outputs of the triboelectric unit exhibit a trend akin to that when $\alpha = 60^\circ$, as shown in Fig. 3d, e. An observable difference is that, for $\alpha = 180^\circ$, the OC-voltage is saturated at around 177 V with the increasing value of θ , which is lower than the saturated voltage of 200 V under a small swing amplitude of $\alpha = 60^\circ$. For a given swing frequency of 4 Hz, the swing speed of the pendulum as driven by the motor grows with the rise of swing amplitude, which contributes to the enhanced spin speed of the rotor, as shown in Fig. 3c, f. Since the high-speed spin of the rotor affects the contact intimacy between the FEP films and electrodes, the saturated OC-voltage is reduced under a large swing amplitude of 180° . Although

the triboelectric effect is slightly weakened under a high spin speed of the rotor, the induced charges flow in the external circuit with a significantly increased speed, engendering high output current $I_{SC} = 3.6 \mu\text{A}$ at $\theta = 60^\circ$ under a large swing amplitude $\alpha = 180^\circ$. Moreover, for $\alpha = 180^\circ$ and $\theta = 0^\circ$, the rotor spins at a speed around 5.7 rps (round per second), which is 142.5% increase as compared with the swing speed (4 rps) of the pendulum. Consequently, the frequency-multiplied output performance of the M-TEHG is enabled by the enhanced spin speed of the rotor.

To exhibit the feasibility of the motion modulation in practical applications where the two-way swing of the pendulum is engendered by external motions, we excited the M-TEHG using a swing arm with a length of $L = 270$ mm and swing amplitude of $\gamma = 20^\circ$ at 4 Hz to observe the output characteristics, as schematically illustrated in Fig. 4a. Owing to the effect of the rotary inertia, the pendulum swings oppositely with respect to the swing arm, resulting in the periodical storage and release of the swing energy of the pendulum through the spiral spring. Similar to the observation when the pendulum is driven directly by a motor, electric outputs of the triboelectric unit in this case also rise from 40 V/1

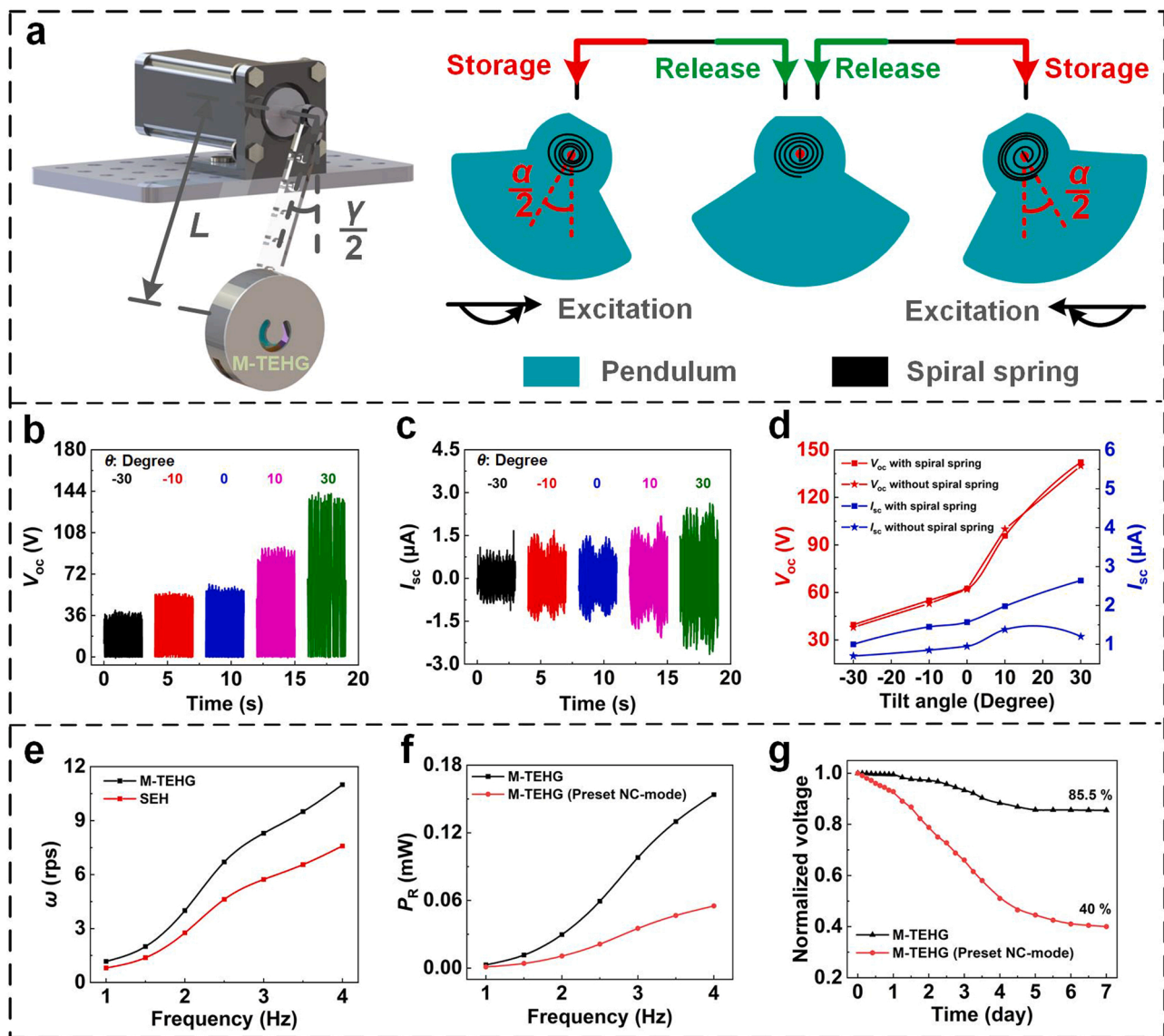


Fig. 4. Demonstration of transforming two-way swing to one-way spin by the MMS when the M-TEHG is driven by a swing arm. (a) Schematic illustration of swing excitation. (b) OC-voltage and (c) SC-current at various tilt angles. (d) OC-voltage and SC-current versus tilt angle. (e) Root-mean-square speeds of the M-TEHG and SEH. (f) Output power of the M-TEHG and the preset NC-mode M-TEHG at various swing frequencies. (g) Durability of the M-TEHG and the preset NC-mode M-TEHG. (e)-(g) were measured under $\theta = 0^\circ$ and $\gamma = 20^\circ$.

μA to $142\text{ V}/2.6\text{ }\mu\text{A}$ with increasing the tilt angle θ from -30° to 30° as the M-TEHG transitions gradually from NC-mode to C-mode, as depicted in Fig. 4b, c. The introduction of the spiral spring to the pendulum does not change the intermittent sliding contact between the FEP films and electrodes and thus has insignificant effect on the output voltage of the triboelectric unit, as shown in Fig. 4d. However, with the spiral spring, the entire stroke energy of the pendulum can be utilized, which contributes to the enhanced spin speed of the rotor and hence enlarged output current from the triboelectric unit as compared with that without the spiral spring. It should be noted that the SC-current without the spiral spring drops when the tilt angle rises from 20° to 30° due to the increased contact force and the resultant friction between the rotor and the electrode. Without the spiral spring, the spin speed of the rotor declines quickly with the increased friction resistance, which lowers the charge transfer speed and hence leads to reduced output current with increasing the tilt angle from 20° to 30° .

Compared with the pendulum speed of a conventional swing energy harvester (SEH), the rotor speed of the M-TEHG is remarkably increased, as shown in Fig. 4e. For this reason, electric outputs of the M-TEHG are almost one order of magnitude higher than those of the SEH, as shown in Fig. S7. If the M-TEHG is designed to work only in C-mode (preset C-mode, i.e., the rotor cannot move along the supporting shaft), the comparatively small driving force of the pendulum cannot overcome the friction drag between the rotor and the electrode layer to generate electricity. Although the M-TEHG can work in the preset NC-mode, both

the OC-voltage and the SC-current are lower than those of the proposed (WMT) M-TEHG, as plotted in Fig. S8. Moreover, thanks to the continual replenishment of triboelectric charges, the output power of the proposed M-TEHG is significantly higher than that of the preset NC-mode M-TEHG, as exhibited in Fig. 4f. The durability of the M-TEHG was also examined by exposing it to a swing motion of 4 Hz for 30 min each day for 7 days , as shown in Fig. 4g. Compared with the preset NC-mode M-TEHG that can only maintain 40% of its electric output, the proposed M-TEHG can retain 85.5% electric output. The M-TEHG also has improved or comparable durability as compared with other designs, as shown in Table S1. The excellent durability of the proposed M-TEHG is attributed to the intermittent and automatic WMT that originates from the tiny motion of the rotor along its axle. The automatic WMT enables the triboelectric unit to regenerate and replenish the dissipated charges at the cost of significantly reduced material abrasion and friction resistance.

When the spin axis of the proposed M-TEHG is parallel to the ground ($\theta = 0^\circ$), the OC-voltage output can persist for 13 s without observable attenuation after the external swing is stopped (Fig. S9). However, the output current decays with the decreasing spin speed of the rotor. For the electromagnetic unit, both the voltage and current attenuate after the external swing is removed since they are positively related to the spin speed of the rotor, as illustrated in Fig. S10. Moreover, the M-TEHG can generate electric outputs at a frequency ($\sim 33\text{ Hz}$) far larger than the excitation frequency (4 Hz), exhibiting frequency-multiplied output

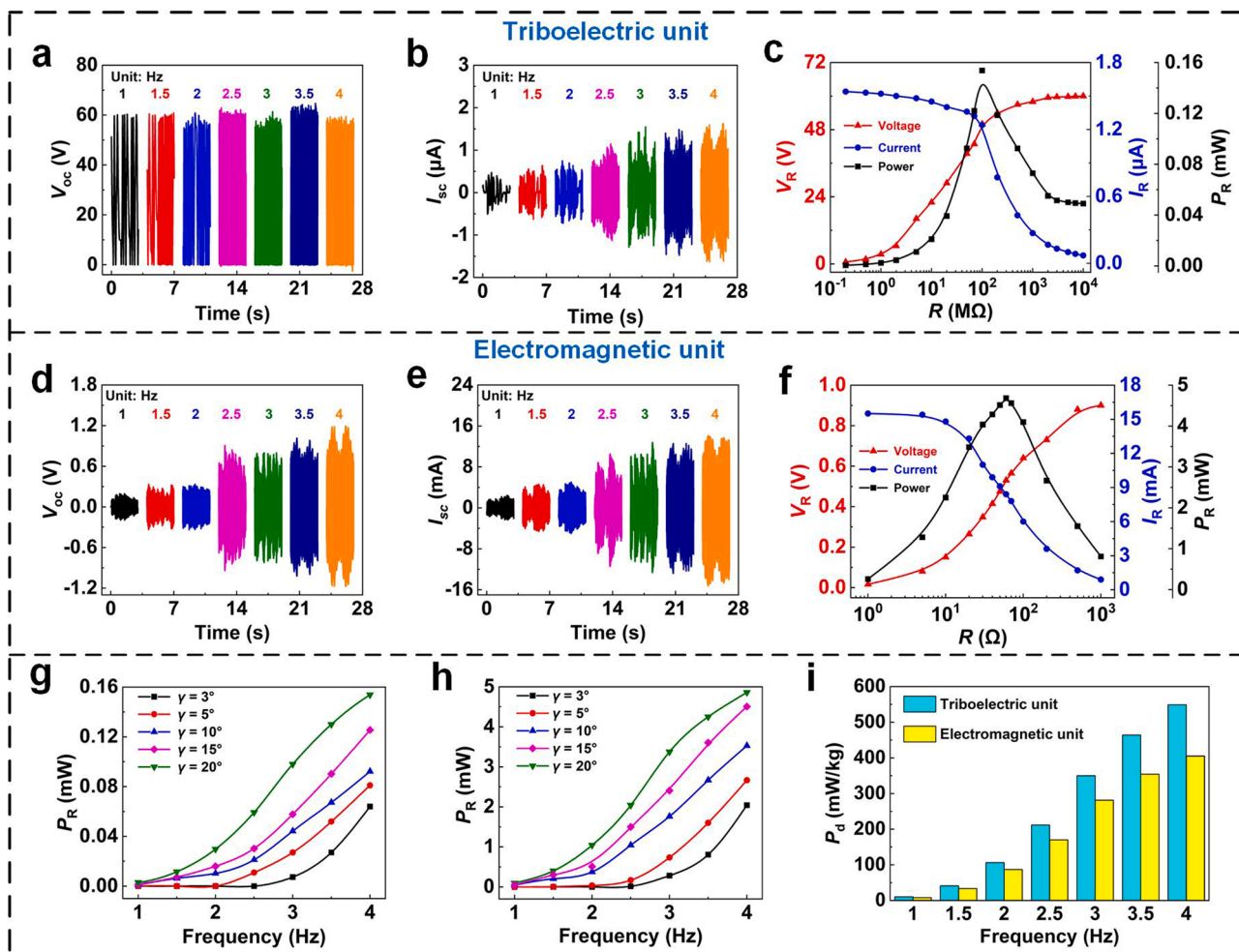


Fig. 5. Output characteristics of the M-TEHG as excited by external swing. (a) OC-voltage and (b) SC-current of the triboelectric unit. (c) Load voltage, current and power of the triboelectric unit versus resistance. (d) OC-voltage and (e) SC-current of the electromagnetic unit. (f) Load voltage, current and power of the electromagnetic unit versus resistance. (g) Output power of the triboelectric unit versus frequency under various swing amplitudes. (h) Output power of the electromagnetic unit versus frequency under various swing amplitudes. (i) Power density at various frequencies.

performance. These tests demonstrate the capability of the MMS in transforming external motions to the one-way and high-speed spin (11 rps) of the rotor. The Supporting Video S2 is also provided to show this motion modulation process.

2.3. Performance of the proposed M-TEHG

The M-TEHG is designed to work normally with its spin axis parallel to the ground (i.e., $\theta = 0^\circ$) to harness ambient low-frequency motions. We first examine the performance of the M-TEHG as excited by external swing with a constant amplitude of $\gamma = 20^\circ$. For the triboelectric unit, the OC-voltage V_{OC} fluctuates slightly around 60 V at various swing frequencies due to the occasional rubbing of the FEP films with the electrodes, whereas the SC-current I_{SC} grows steadily from 0.5 μA to 1.6 μA as the swing frequency ascends from 1 to 4 Hz, as illustrated in Fig. 5a, b. The steady growth of I_{SC} is ascribed to the increased spin speed of the rotor with the swing frequency, which drives the charges to flow between the two electrodes with enhanced speeds via the external circuit. For a given swing frequency of 4 Hz, the load voltage V_R ascends but the load current I_R descends with an increase in the resistance, as plotted in Fig. 5c. The optimal instantaneous power of $P_R = 0.15$ mW is achieved with a load of 100 M Ω , corresponding to a high power density of 549 mW/kg. For the electromagnetic unit, the OC-voltage V_{OC} and

SC-current I_{SC} rise from 0.2 V/2.6 mA to 1.2 V/14.1 mA in the spectral region from 1 to 4 Hz, as depicted in Fig. 5d, e. The load voltage V_R and load current I_R also exhibit opposite variation trends with an increase in the resistance, as depicted in Fig. 5f. The maximum power ($P_R = 4.7$ mW) of the electromagnetic unit is acquired with a load of 60 Ω , indicating a low power density (405 mW/kg) as compared with that (549 mW/kg) of the triboelectric unit. Except the swing frequency, increasing the swing amplitude can also boost electric outputs of the two units as more kinetic energy is input into the M-TEHG, as shown in Fig. S11. Frequency responses of the output power of the two units under various swing amplitudes are depicted in Fig. 5g, h. Although the triboelectric unit has relatively low output power, its power density distinctly outperforms that of the electromagnetic unit at various swing frequencies, as shown in Fig. 5i. When working as a two-channel power source, the watch-sized M-TEHG can provide high OC-voltage of 60 V and optimal power of 0.15 mW from the triboelectric unit, and large SC-current of 14 mA and optimal power of 4.7 mW from the electromagnetic unit as excited at 4 Hz by the external swing with $\gamma = 20^\circ$.

In addition to swings, the M-TEHG can also convert low-frequency vibrations into electricity, as illustrated in Fig. 6a. This test was also conducted with the spin axis of the M-TEHG parallel to the ground. For a constant vibration amplitude of 25 mm, V_{OC} of the triboelectric unit maintains in the proximity of 64 V at various vibration frequencies as a

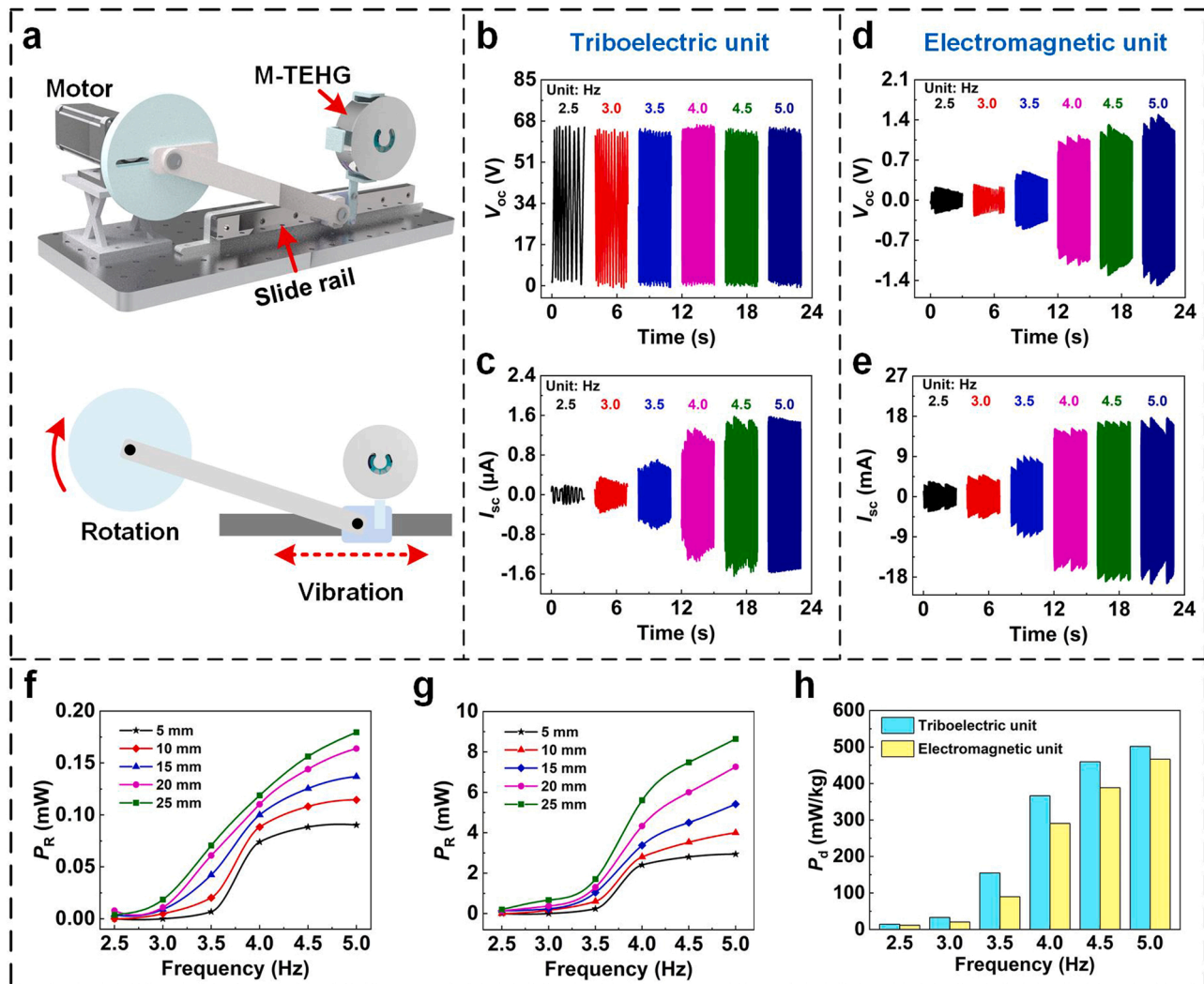


Fig. 6. Output characteristics of the M-TEHG as excited by vibration. (a) Schematic illustration of the test. (b) OC-voltage and (c) SC-current of the triboelectric unit. (d) OC-voltage and (e) SC-current of the electromagnetic unit. (f) Output power of the triboelectric unit versus frequency. (g) Output power of the electromagnetic unit versus frequency. (h) Power density at various frequencies.

result of the occasional rubbing of the FEP films with the electrodes, as exhibited in Fig. 6b. With an increase in the vibration frequency from 2.5 to 5 Hz, I_{SC} of the triboelectric unit goes up from 0.2 μA to 1.6 μA owing to the ever increasing spin speed of the rotor with the frequency under a constant vibration amplitude, as plotted in Fig. 6c. Since the electric outputs of the electromagnetic unit are positively related to the spin speed of the rotor, its V_{OC} and I_{SC} rise from 0.3 V/3.6 mA to 1.5 V/17.6 mA as the vibration frequency varies from 2.5 to 5 Hz, as shown in Fig. 6d, e. The vibration amplitude has a similar effect on the electric outputs of the M-TEHG, i.e., apart from the voltage of the triboelectric unit that keeps nearly unchanged, other outputs of the two units grow gradually with the increasing amplitude from 5 mm to 25 mm, as shown in Fig. S12. Power outputs of the triboelectric unit and electromagnetic unit ascend with both the vibration amplitude and frequency. Under the vibration amplitude of 25 mm, the triboelectric unit generates 0.18 mW power and the electromagnetic unit outputs 8.6 mW at 5 Hz, as shown in Fig. 6f, g. The power density of the two units versus the vibration frequency is shown in Fig. 6h, which are obtained under a constant vibration amplitude of 15 mm and highlight the superior performance of the triboelectric unit in scavenging low-frequency (< 5 Hz) vibration energy. This test reveals the excellent performance of the M-TEHG in tapping low-frequency vibrations.

Water waves are a kind of rich and renewable energy source, but its utilization still faces high challenge due to the low-frequency and irregular nature. The M-TEHG may be a potential technology for the exploitation of water waves since it can transform low-frequency motions to one-way spin. To test this hypothesis, we put the M-TEHG in a floating box with an inner length $x = 120$ mm to receive the water waves produced by a water pump, as schematically illustrated in Fig. 7a. Owing to the intermittent rubbing between the FEP films and electrodes caused by the irregular water waves, V_{OC} of the triboelectric unit can stabilize at around 60 V as the wave frequency rises from 0.7 to 1.0 Hz (Fig. 7b). However, I_{SC} of the triboelectric unit goes up steadily with the rising wave frequency, which is enabled by the increased rotor speed with the elevated wave frequency, as exhibited in Fig. 7c. Due to the same cause, V_{OC} and I_{SC} of the electromagnetic unit also grow continuously from 0.2 V/3.2 mA to 0.5 V/9.6 mA with increasing the wave frequency from 0.7 to 1.0 Hz, as plotted in Fig. 7d, e. The output power of the watch-sized M-TEHG ascends quickly with the wave frequency, as shown in Fig. 7f, g. The power of the triboelectric unit reaches 0.023 mW at 1.0 Hz, corresponding to a relatively high power density of 84 mW/kg, which is higher than that (58 mW/kg) of the electromagnetic unit at the same wave frequency, as plotted in Fig. 7h. From these measurements, the application of the M-TEHG in harnessing water

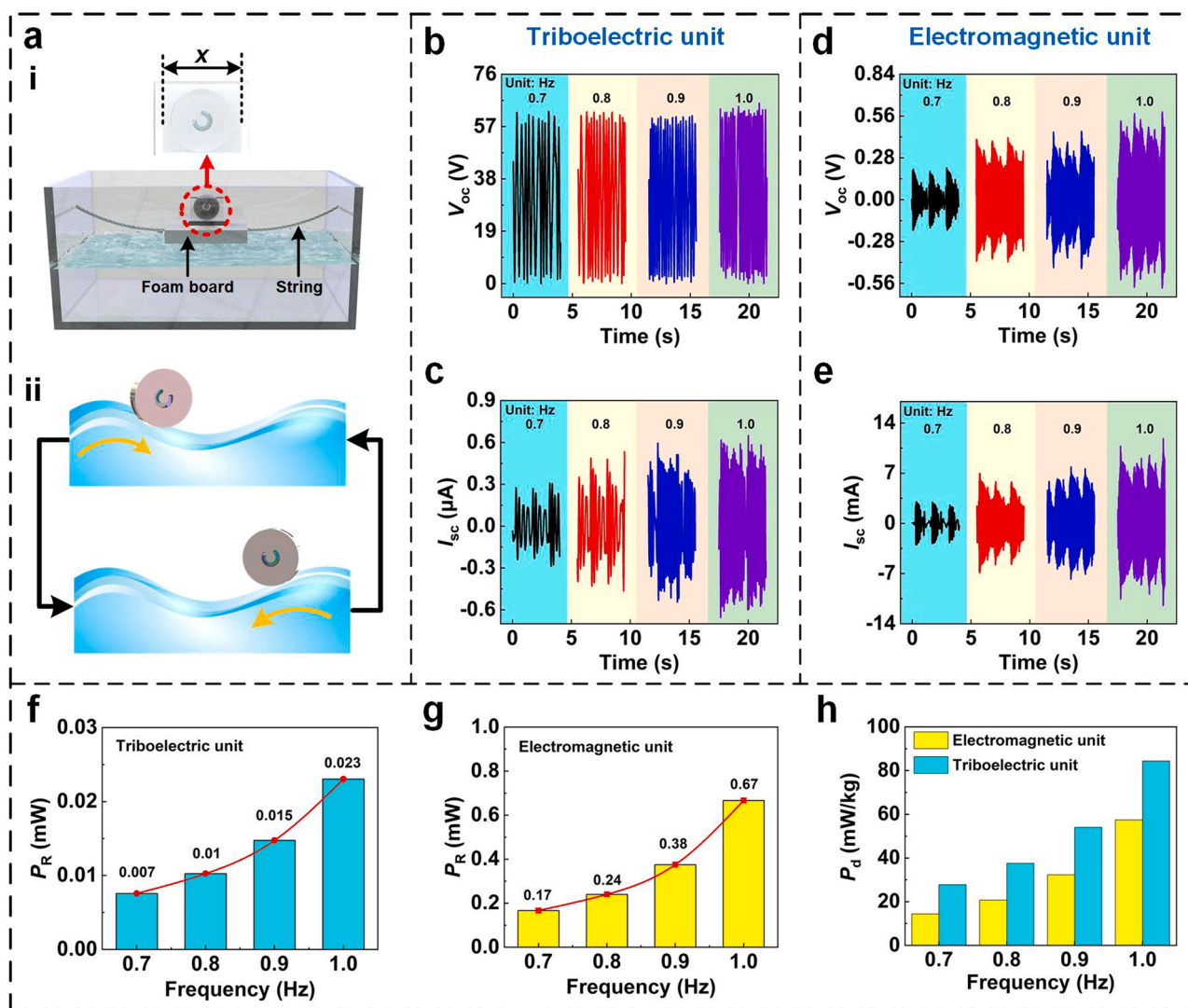


Fig. 7. Output characteristics of the M-TEHG as excited by water wave. (a) Schematic illustration of the test. (b) OC-voltage and (c) SC-current of the triboelectric unit. (d) OC-voltage and (e) SC-current of the electromagnetic unit. (f) Output power of the triboelectric unit versus frequency. (g) Output power of the electromagnetic unit versus frequency. (h) Power density at various frequencies.

waves or blue energy (ocean waves) is highly possible.

2.4. Application demonstration of the M-TEHG

To explore the capability of the M-TEHG in harnessing ambient low-frequency motions as a practical power source, it was first used to charge a $3.3\ \mu\text{F}$ capacitor with the energy captured from the swing motion with an amplitude of 20° and frequency of 4 Hz through a power management circuit, as shown in Fig. 8a. Consisting of two bridge rectifiers, the power management circuit separately converts the alternating-current (AC) outputs of the triboelectric unit and the electromagnetic unit to direct-current (DC) outputs before charging the capacitor or being connected in parallel as the M-TEHG output, as illustrated in Fig. S13. With the high output current but low output voltage, the electromagnetic unit can lift the voltage of the capacitor to the saturated level of 0.07 V in 0.7 s. The low saturated voltage but fast charging process of the electromagnetic unit provides a platform, on which the voltage of the capacitor can be increased more quickly by the triboelectric unit. Working as a whole, the M-TEHG can generate electricity out of the low-frequency swing to charge various capacitors and light up 120 LEDs, as shown in Fig. 8b, c and Supporting Video S3.

When attached to human arms, the watch-sized M-TEHG can convert sufficient electric energy from the swings of human arms to sustainably power a wearable electronic watch, as pictured in Fig. 8d and recorded in Supporting Video S4. In this test, a fully discharged capacitor ($100\ \mu\text{F}$) is first charged to 1.26 V by the M-TEHG in 60 s and then connected to the electronic watch. The slight fluctuation in the voltage of the capacitor around 1.2 V indicates that the M-TEHG can maintain the normal work of the watch with the energy converted from the human arm swing, as illustrated in Fig. 8e. When the M-TEHG is set in a small floating box and triggered by the water waves produced by a water pump at 0.9 Hz, the generator can charge a fully discharged capacitor ($100\ \mu\text{F}$) to 1.9 V in less than 10 min, and the stored electric energy can drive a hygrometer to work for 5 s, as pictured in Fig. 8f and exhibited in

Supporting Video S5. Under the same condition, the M-TEHG can also light up 66 LEDs that form the word ‘TENG’, as displayed in Fig. S14 and Supporting Video S6. These tests clearly demonstrate the superior capability of the M-TEHG in tapping ambient low-frequency and irregular motions and its promising applications in self-sufficient electronic devices.

Supplementary material related to this article can be found online at [doi:10.1016/j.nanoen.2022.107867](https://doi.org/10.1016/j.nanoen.2022.107867).

Supplementary material related to this article can be found online at [doi:10.1016/j.nanoen.2022.107867](https://doi.org/10.1016/j.nanoen.2022.107867).

Supplementary material related to this article can be found online at [doi:10.1016/j.nanoen.2022.107867](https://doi.org/10.1016/j.nanoen.2022.107867).

3. Conclusions

In summary, this paper presents a fundamentally different mechanical motion-controlled switch to transform various low-frequency and irregular motions to one-way and high-speed spin. With the proposed switch, a watch-sized M-TEHG was conceived and fabricated, which can automatically switch between NC-mode and C-mode by taking advantage of the irregularity of ambient motions to maintain high electrical stability. A series of experimental tests have been carried out to reveal the superior performance of the M-TEHG in harnessing low-frequency swings, vibrations, and water waves. When the watch-sized M-TEHG is excited by low-frequency (≤ 5 Hz) swings and vibrations, it can generate milliwatt-level electric power. The output power of the M-TEHG can reach approximately 0.7 mW when it is exposed to irregular water waves of 1 Hz. By exploiting human limb swings and water waves, the watch-sized M-TEHG can sustain the normal work of an electronic watch, drive a hygrometer, and light up dozens of LEDs. Working on the basis of triboelectric effect (interfacial effect), the output power of the triboelectric unit in the watch-sized M-TEHG is comparatively low, but it can be significantly improved by enlarging the rotor diameter or employing multi-layered rotor structure to increase the interfacial area

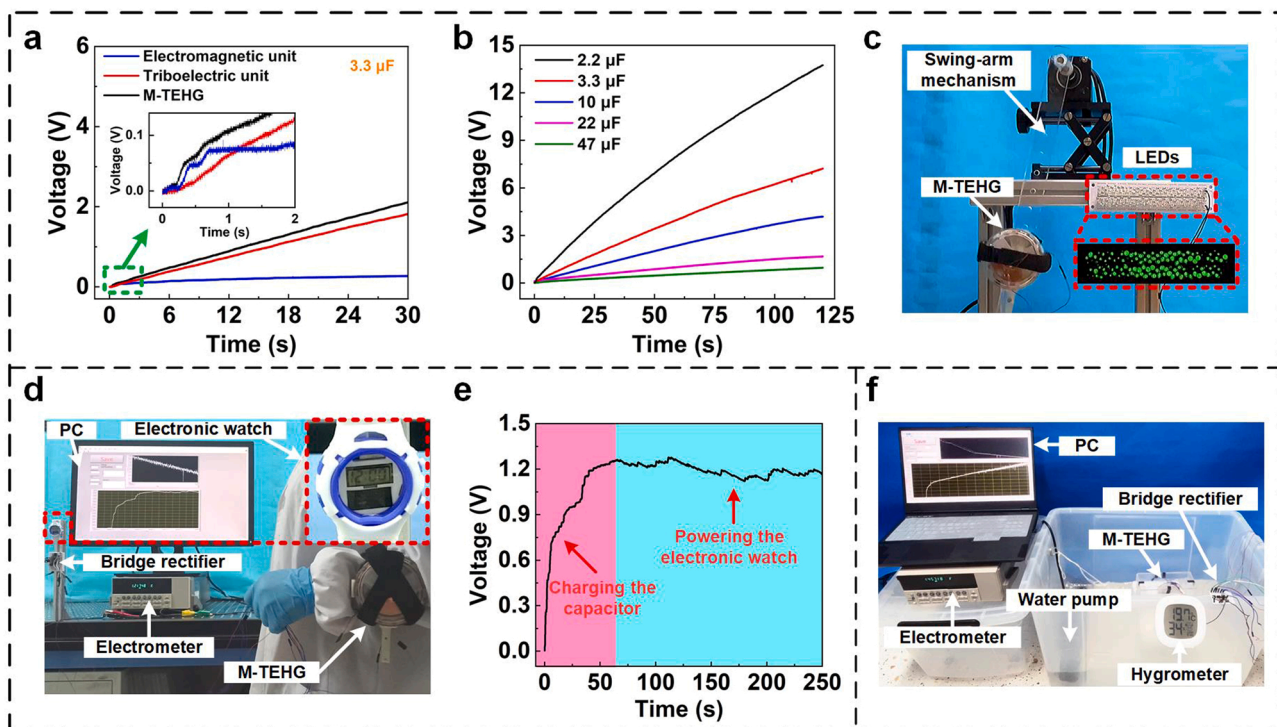


Fig. 8. Application demonstration of the M-TEHG. (a) Voltage curves of a $3.3\ \mu\text{F}$ capacitor as charged by the triboelectric unit, electromagnetic unit, and M-TEHG. (b) Voltage curves of multiple capacitors as charged by the M-TEHG. (c) Photograph of harvesting swing motion of 20° at 1.5 Hz by the M-TEHG for lighting up 120 LEDs. (d) Photograph of harnessing human arm swings by the M-TEHG for driving an electronic watch. (e) Charging and discharging process of a $100\ \mu\text{F}$ capacitor in powering the electronic watch. (f) Photograph of harnessing water wave of 0.9 Hz by the M-TEHG for driving a hygrometer.

of the triboelectric unit. Given the frequency-multiplied output performance, high mechanical durability, high electrical stability, and superior adaptability (to various motions), the M-TEHG proposed in this study can serve as a practical power source for self-sufficient sensing systems and wearable electronics by exploiting ambient low-frequency and renewable mechanical energy.

4. Experimental section

4.1. Fabrication of the pendulum

The pendulum consists of a fan-shaped eccentric substrate and seven tuned mass blocks. The eccentric substrate (central angle: 140°, thickness: 5 mm) was made by 3D printing technology from non-transparent UV Curable Resin. The seven cylindrical mass blocks were made of copper, four of which have a size of $\Phi 6 \text{ mm} \times 5 \text{ mm}$ and the other three have a size of $\Phi 3 \text{ mm} \times 5 \text{ mm}$. The cantilevered plectrum includes a PET layer and a copper layer. The PET layer has a size of $25 \text{ mm} \times 4 \text{ mm} \times 0.1 \text{ mm}$ and the copper layer has a size of $22 \text{ mm} \times 4 \text{ mm} \times 0.2 \text{ mm}$.

4.2. Fabrication of the rotor

The rotor is composed of a circular substrate, three pieces of fan-shaped FEP films, and sixteen cuboidal magnets (Nd-Fe-B). The circular substrate was also prepared by 3D printing technology with jagged inner wall, which is 10 mm in thickness and 66 mm in diameter. The FEP films each has a central angle of 60°, inner radius of 10 mm, and outer radius of 33 mm. The sixteen cuboidal magnets have the same dimension of $8 \text{ mm} \times 3 \text{ mm} \times 1 \text{ mm}$.

4.3. Fabrication of the stator

For the electromagnetic unit, the stator includes sixteen sets of coils that were made of varnished wire with a diameter of 0.14 mm. Connected in series, all the coils have a resistance of 60 Ω . For the triboelectric unit, the stator is comprised of two complementary copper electrodes. Each of the two electrodes includes three fan-shaped copper foils with an inner radius of 8.5 mm, outer radius of 33 mm, and central angle of around 55°.

4.4. Assemblage of the M-TEHG

The pendulum, rotor, and electrode layer were coaxially mounted using two ceramic bearings and a bronze shaft. Of the two bearings, one has a small size (inner diameter: 5 mm, outer diameter: 11 mm, and thickness: 4 mm) for assembling the pendulum, and the other has a large size (inner diameter: 8 mm, outer diameter: 16 mm, and thickness: 5 mm) for connecting the rotor to the shaft. The shaft for supporting the rotor has a diameter of 7.9 mm, leaving about 0.1 mm interstice between the shaft and the larger bearing to enable the motion of the rotor along the spin axis. The stainless steel spiral spring with a width of 2.5 mm was mounted between the pendulum and the lid. All components of the M-TEHG were packaged in a cylindrical housing made of transparent UV Curable Resin. The assembled M-TEHG is 79 mm in diameter and 25.5 mm in thickness.

4.5. Electrical measurement

The low-frequency swings and vibrations were respectively provided by a customized swing arm and a crank-slider mechanism that were all driven by a stepper motor (DE60HB102–1000, DVS Mechatronics, China) with adjustable frequency and speed. The water waves were produced by a water pump (SCP-180, 65 W). The voltage, current and charge outputs of the M-TEHG in different tests were measured using an electrometer (6514, Keithley, USA).

CRedit authorship contribution statement

Yan Zhang: Investigation, Data curation, Formal analysis, Writing – original draft. **Kangqi Fan:** Conceptualization, Supervision, Writing – original draft. **Jiuling Zhu:** Methodology, Validation. **Shuxin Wu:** Investigation, Software. **Sheng Zhang:** Project administration, Visualization. **Tinghai Cheng:** Conceptualization, Resources, Writing – review & editing, Supervision. **Zhong Lin Wang:** Conceptualization, Resources, Writing – review & editing, Supervision.

Declaration of Competing Interest

The authors declare that they have no known competing financial interests or personal relationships that could have appeared to influence the work reported in this paper.

Data availability

Data will be made available on request.

Acknowledgments

This research is supported by the National Natural Science Foundation of China (No. 52077159), the National Key Research and Development Project from the Ministry of Science and Technology (Nos. 2021YFA1201601 & 2021YFA1201604), and the Natural Science Foundation of Beijing Municipality (No. 3222023).

Appendix A. Supplementary material

Supplementary data associated with this article can be found in the online version at [doi:10.1016/j.nanoen.2022.107867](https://doi.org/10.1016/j.nanoen.2022.107867).

References

- [1] Z.L. Wang, From contact electrification to triboelectric nanogenerators, *Rep. Prog. Phys.* 84 (2021), 096502.
- [2] J. Wang, W. Ding, L. Pan, C. Wu, H. Yu, L. Yang, R. Liao, Z.L. Wang, Self-powered wind sensor system for detecting wind speed and direction based on a triboelectric nanogenerator, *ACS Nano* 12 (2018) 3954–3963.
- [3] Z.L. Wang, Triboelectric nanogenerators as new energy technology and self-powered sensors – principles, problems and perspectives, *Faraday Discuss.* 176 (2014) 447–458.
- [4] Z.L. Wang, Entropy theory of distributed energy for internet of things, *Nano Energy* 58 (2019) 669–672.
- [5] Z. Yang, S. Zhou, J. Zu, D. Inman, High-performance piezoelectric energy harvesters and their applications, *Joule* 2 (2018) 642–697.
- [6] K. Fan, J. Liu, M. Cai, M. Zhang, T. Qiu, L. Tang, Exploiting ultralow-frequency energy via vibration-to-rotation conversion of a rope-spun rotor, *Energ. Convers. Manag.* 225 (2020), 113433.
- [7] Q. Tang, M.-H. Yeh, G. Liu, S. Li, J. Chen, Y. Bai, L. Feng, M. Lai, K.-C. Ho, H. Guo, C. Hu, Whirligig-inspired triboelectric nanogenerator with ultrahigh specific output as reliable portable instant power supply for personal health monitoring devices, *Nano Energy* 47 (2018) 74–80.
- [8] H. Liu, J. Zhong, C. Lee, S.-W. Lee, L. Lin, A comprehensive review on piezoelectric energy harvesting technology: materials, mechanisms, and applications, *Appl. Phys. Rev.* 5 (2018), 041306.
- [9] L. Costanzo, M. Liu, A.L. Schiavo, M. Vitelli, L. Zuo, Backpack energy harvesting system with maximum power point tracking capability, *IEEE Trans. Ind. Electron.* 69 (2022) 506–516.
- [10] C. Zhang, W. Tang, C. Han, F. Fan, Z.L. Wang, Theoretical comparison, equivalent transformation, and conjunction operations of electromagnetic induction generator and triboelectric nanogenerator for harvesting mechanical energy, *Adv. Mater.* 26 (2014) 3580–3591.
- [11] Z.L. Wang, Catch wave power in floating nets, *Nature* 542 (2017) 159–160.
- [12] Z. Wu, B. Zhang, H. Zou, Z. Lin, G. Liu, Z.L. Wang, Multifunctional sensor based on translational-rotary triboelectric nanogenerator, *Adv. Energy Mater.* 9 (2019) 1901124.
- [13] T. Lin, Y. Pan, S. Chen, L. Zuo, Modeling and field testing of an electromagnetic energy harvester for rail tracks with anchorless mounting, *Appl. Energy* 213 (2018) 219–226.
- [14] F.-R. Fan, Z.-Q. Tian, Z. Lin Wang, Flexible triboelectric generator, *Nano Energy* 1 (2012) 328–334.

- [15] Z. Lin, B. Zhang, H. Guo, Z. Wu, H. Zou, J. Yang, Z.L. Wang, Super-robust and frequency-multiplied triboelectric nanogenerator for efficient harvesting water and wind energy, *Nano Energy* 64 (2019), 103908.
- [16] Z. Zhou, L. Weng, T. Tat, A. Libanori, Z. Lin, L. Ge, J. Yang, J. Chen, Smart insole for robust wearable biomechanical energy harvesting in harsh environments, *ACS Nano* 14 (2020) 14126–14133.
- [17] N. Zheng, J. Xue, Y. Jie, X. Cao, Z.L. Wang, Wearable and humidity-resistant biomaterials-based triboelectric nanogenerator for high entropy energy harvesting and self-powered sensing, *Nano Res.* 15 (2022) 6213–6219.
- [18] Z.L. Wang, On Maxwell's displacement current for energy and sensors: The origin of nanogenerators, *Mater. Today* 20 (2017) 74–82.
- [19] Y. Chen, Y. Jie, N. Wang, Z.L. Wang, X. Cao, Novel wireless power transmission based on Maxwell displacement current, *Nano Energy* 76 (2020), 105051.
- [20] J. Chen, H. Guo, Z. Wu, G. Xu, Y. Zi, C. Hu, Z.L. Wang, Actuation and sensor integrated self-powered cantilever system based on TENG technology, *Nano Energy* 64 (2019), 103920.
- [21] H. Yang, Y. Pang, T. Bu, W. Liu, J. Luo, D. Jiang, C. Zhang, Z.L. Wang, Triboelectric micromotors actuated by ultralow frequency mechanical stimuli, *Nat. Commun.* 10 (2019) 2309.
- [22] B. Cheng, Q. Xu, Y. Ding, S. Bai, X. Jia, Y. Yu, J. Wen, Y. Qin, High performance temperature difference triboelectric nanogenerator, *Nat. Commun.* 12 (2021) 4782.
- [23] Y. Hu, J. Yang, S. Niu, W. Wu, Z.L. Wang, Hybridizing triboelectrification and electromagnetic induction effects for high-efficient mechanical energy harvesting, *ACS Nano* 8 (2014) 7442–7450.
- [24] G. Zhu, J. Chen, T. Zhang, Q. Jing, Z.L. Wang, Radial-arrayed rotary electrification for high performance triboelectric generator, *Nat. Commun.* 5 (2014) 3426.
- [25] K. Tao, Z. Chen, H. Yi, R. Zhang, Q. Shen, J. Wu, L. Tang, K. Fan, Y. Fu, J. Miao, W. Yuan, Hierarchical honeycomb-structured electret/triboelectric nanogenerator for biomechanical and morphing wing energy harvesting, *Nano-Micro Lett.* 13 (2021) 123.
- [26] J. Wang, Y. Cao, H. Xiang, Z. Zhang, J. Liang, X. Li, D. Ding, T. Li, L. Tang, A piezoelectric smart backing ring for high-performance power generation subject to train induced steel-spring fulcrum forces, *Energy Convers. Manag.* 257 (2022), 115442.
- [27] Y. Gao, G. Liu, T. Bu, Y. Liu, Y. Qi, Y. Xie, S. Xu, W. Deng, W. Yang, C. Zhang, Mxene based mechanically and electrically enhanced film for triboelectric nanogenerator, *Nano Res.* 14 (2021) 4833–4840.
- [28] Q. He, Y. Wu, Z. Feng, C. Sun, W. Fan, Z. Zhou, K. Meng, E. Fan, J. Yang, Triboelectric vibration sensor for a human-machine interface built on ubiquitous surfaces, *Nano Energy* 59 (2019) 689–696.
- [29] Q. Gao, T. Cheng, Z.L. Wang, Triboelectric mechanical sensors—progress and prospects, *Extrem. Mech. Lett.* 42 (2021), 101100.
- [30] N. Li, Z. Yin, W. Zhang, C. Xing, T. Peng, B. Meng, J. Yang, Z. Peng, A triboelectric-inductive hybrid tactile sensor for highly accurate object recognition, *Nano Energy* 96 (2022), 107063.
- [31] Y. Feng, T. Jiang, X. Liang, J. An, Z.L. Wang, Cylindrical triboelectric nanogenerator based on swing structure for efficient harvesting of ultra-low-frequency water wave energy, *Appl. Phys. Rev.* 7 (2020), 021401.
- [32] T. Jiang, H. Pang, J. An, P. Lu, Y. Feng, X. Liang, W. Zhong, Z.L. Wang, Robust swing-structured triboelectric nanogenerator for efficient blue energy harvesting, *Adv. Energy Mater.* 10 (2020) 2000064.
- [33] Z. Wu, H. Guo, W. Ding, Y.-C. Wang, L. Zhang, Z.L. Wang, A hybridized triboelectric–electromagnetic water wave energy harvester based on a magnetic sphere, *ACS Nano* (2019).
- [34] L. Long, W. Liu, Z. Wang, W. He, G. Li, Q. Tang, H. Guo, X. Pu, Y. Liu, C. Hu, High performance floating self-excited sliding triboelectric nanogenerator for micro mechanical energy harvesting, *Nat. Commun.* 12 (2021) 4689.
- [35] Z. Lin, B. Zhang, H. Zou, Z. Wu, H. Guo, Y. Zhang, J. Yang, Z.L. Wang, Rationally designed rotation triboelectric nanogenerators with much extended lifetime and durability, *Nano Energy* 68 (2020), 104378.
- [36] Z. Lin, B. Zhang, Y. Xie, Z. Wu, J. Yang, Z.L. Wang, Elastic-connection and soft-contact triboelectric nanogenerator with superior durability and efficiency, *Adv. Funct. Mater.* 31 (2021) 2105237.
- [37] J. Han, Y. Feng, P. Chen, X. Liang, H. Pang, T. Jiang, Z.L. Wang, Wind-driven soft-contact rotary triboelectric nanogenerator based on rabbit fur with high performance and durability for smart farming, *Adv. Funct. Mater.* 32 (2022) 2108580.
- [38] H. Pang, Y. Feng, J. An, P. Chen, J. Han, T. Jiang, Z.L. Wang, Segmented swing-structured fur-based triboelectric nanogenerator for harvesting blue energy toward marine environmental applications, *Adv. Funct. Mater.* 31 (2021) 2106398.
- [39] J. Chen, H. Guo, C. Hu, Z.L. Wang, Robust triboelectric nanogenerator achieved by centrifugal force induced automatic working mode transition, *Adv. Energy Mater.* 10 (2020) 2000886.
- [40] K. Fan, D. Wei, Y. Zhang, P. Wang, K. Tao, R. Yang, A whirligig-inspired intermittent-contact triboelectric nanogenerator for efficient low-frequency vibration energy harvesting, *Nano Energy* 90 (2021), 106576.
- [41] K. Zhang, X. Wang, Y. Yang, Z.L. Wang, Hybridized electromagnetic-triboelectric nanogenerator for scavenging biomechanical energy for sustainably powering wearable electronics, *ACS Nano* 9 (2015) 3521–3529.
- [42] Y. Wu, X. Wang, Y. Yang, Z.L. Wang, Hybrid energy cell for harvesting mechanical energy from one motion using two approaches, *Nano Energy* 11 (2015) 162–170.
- [43] X. Zhong, Y. Yang, X. Wang, Z.L. Wang, Rotating-disk-based hybridized electromagnetic-triboelectric nanogenerator for scavenging biomechanical energy as a mobile power source, *Nano Energy* 13 (2015) 771–780.
- [44] B. Kathalia, D. Tan, I. Stern, A. Erturk, An experimentally validated model for geometrically nonlinear plucking-based frequency up-conversion in energy harvesting, *Smart Mater. Struct.* 27 (2017), 015024.
- [45] H. Zou, L. Guo, H. Xue, Y. Zhang, X. Shen, X. Liu, P. Wang, X. He, G. Dai, P. Jiang, H. Zheng, B. Zhang, C. Xu, Z.L. Wang, Quantifying and understanding the triboelectric series of inorganic non-metallic materials, *Nat. Commun.* 11 (2020) 2093.
- [46] P. Wang, L. Pan, J. Wang, M. Xu, G. Dai, H. Zou, K. Dong, Z.L. Wang, An ultra-low-friction triboelectric–electromagnetic hybrid nanogenerator for rotation energy harvesting and self-powered wind speed sensor, *ACS Nano* 12 (2018) 9433–9440.
- [47] H. Wu, S. Wang, Z. Wang, Y. Zi, Achieving ultrahigh instantaneous power density of 10 mw/m² by leveraging the opposite-charge-enhanced transistor-like triboelectric nanogenerator (oct-teng), *Nat. Commun.* 12 (2021) 5470.
- [48] B. Zhang, S. Zhang, W. Li, Q. Gao, D. Zhao, Z.L. Wang, T. Cheng, Self-powered sensing for smart agriculture by electromagnetic–triboelectric hybrid generator, *ACS Nano* 15 (2021) 20278–20286.
- [49] H.-X. Zou, L.-C. Zhao, Q.-H. Gao, L. Zuo, F.-R. Liu, T. Tan, K.-X. Wei, W.-M. Zhang, Mechanical modulations for enhancing energy harvesting: principles, methods and applications, *Appl. Energy* 255 (2019), 113871.
- [50] K. Fan, J. Hao, C. Wang, C. Zhang, W. Wang, F. Wang, An eccentric mass-based rotational energy harvester for capturing ultralow-frequency mechanical energy, *Energy Convers. Manag.* 241 (2021), 114301.
- [51] M.A. Halim, R. Rantz, Q. Zhang, L. Gu, K. Yang, S. Roundy, An electromagnetic rotational energy harvester using sprung eccentric rotor, driven by pseudo-walking motion, *Appl. Energy* 217 (2018) 66–74.
- [52] P. Pillatsch, E.M. Yeatman, A.S. Holmes, A piezoelectric frequency up-converting energy harvester with rotating proof mass for human body applications, *Sens. Actuators A* 206 (2014) 178–185.



Yan Zhang received the B.Eng. degree in Electrical Engineering and Automation from Xidian University in 2020. She is currently pursuing her M.S. degree at Xidian University. She is also a visiting student at Beijing Institute of Nanoenergy and Nanosystems. Her research interests are environmental energy harvesting, triboelectric nanogenerators, and self-powered sensors.



Prof. Kangqi Fan received his B.Eng., M.Eng. and Ph.D. degrees from Xidian University in 2002, 2005 and 2007, respectively. He was a visiting scholar at Kansas State University from 2011 to 2012, and a visiting professor at University of Alberta from 2014 to 2015. He is currently a professor with the School of Mechano-Electronic Engineering of Xidian University. He is also a visiting scholar at Beijing Institute of Nanoenergy and Nanosystems. His research interests include triboelectric nanogenerators, energy harvesting, and self-powered sensors.



Jiuling Zhu received the B.Eng. degree in Electrical Engineering and Automation from Xidian University in 2022. He is currently working for his M.S. degree at Xidian University. His research interests focus on triboelectric nanogenerators, biomechanical energy harvesting, and self-powered sensors.



Shuxin Wu received the B.Eng. degree in Electrical Engineering and Automation from Xidian University in 2022. He is currently pursuing his M.S. degree at Xidian University. His research interests are triboelectric nanogenerators, power management circuits, and self-powered sensors.



Prof. Tinghai Cheng received the B.S., M.S. and Ph.D. degrees from Harbin Institute of Technology in 2006, 2008 and 2013, respectively. He was a visiting scholar in the School of Materials Science and Engineering at Georgia Institute of Technology from 2017 to 2018. Currently, he is a professor of Beijing Institute of Nanoenergy and Nanosystems, Chinese Academy of Sciences, and CUSTech Institute of Technology (Wenzhou). His research interests are triboelectric nanogenerators, piezoelectric energy harvesters, and piezoelectric actuators.



Sheng Zhang majored in Materials Science and received the M. S. degree from China University of Mining and Technology in 2020. He is currently studying for his Ph.D. degree in Beijing Institute of Nanoenergy and Nanosystems, Chinese Academy of Sciences, China. His research interests focus on triboelectric nanogenerators and soft robots.



Prof. Zhong Lin Wang received his Ph.D. from Arizona State University in physics. He is now the Hightower Chair in Materials Science and Engineering, Regents' Professor, Engineering Distinguished Professor and Director, Center for Nanostructure Characterization, at Georgia Tech. Dr. Wang has made original and innovative contributions to the synthesis, discovery, characterization and understanding of fundamental physical properties of oxide nanobelts and nanowires, as well as applications of nanowires in energy sciences, electronics, optoelectronics and biological science. His discovery and breakthroughs in developing nanogenerators established the principle and technological road map for harvesting mechanical energy from environment and biological systems for powering personal electronics. His research on self-powered nanosystems has inspired the worldwide effort in academia and industry for studying energy for micro-nano-systems, which is now a distinct disciplinary in energy research and future sensor networks. He coined and pioneered the field of piezotronics and piezophotonics by introducing piezoelectric potential gated charge transport process in fabricating new electronic and optoelectronic devices. Details can be found at: <http://www.nanoscience.gatech.edu>.